Journal of Volcanology and Geothermal Research 298 (2015) 15–26

Contents lists available at ScienceDirect

Journal of Volcanology and Geothermal Research

journal homepage: www.elsevier.com/locate/jvolgeores

Estimation of locations and migration of debris flows on Izu-Oshima Island, Japan, on 16 October 2013 by the distribution of high frequency seismic amplitudes

Masashi Ogiso [a,*], Kiyoshi Yomogida [b]

[a] Meteorological Research Institute, Japan Meteorological Agency, Nagamine 1-1, Tsukuba-city, Ibaraki 305-0052, Japan
[b] Earth and Planetary Dynamics, Graduate School of Science, Hokkaido University, North 10, West 8, Kita-ku, Sapporo 060-0810, Japan

ARTICLE INFO

Article history:
Received 18 September 2014
Accepted 30 March 2015
Available online 7 April 2015

Keywords:
Seismic amplitude
Debris flow
Location estimation
Spatial migration
Scattering

ABSTRACT

In the early morning on 16 October 2013, large debris flows resulted in over 30 people dead on Izu-Oshima Island, Japan, which were induced by heavy rainfall from the approaching Typhoon 1326 (Wipha). We successfully estimated the locations and migration processes of five large events of the debris flows, using the spatial distribution of high-frequency seismic amplitudes recorded by a seismic network on the island. The flows occurred on the western flank of the island, almost at the same place as the site where large traces of debris flows were identified after the disaster. During each event of debris flows, the estimated locations migrated downstream with increasing time, from the caldera rim of Miharayama volcano in the center of the island to its western side with a speed of up to 30 m/s. The estimated time series of source amplitudes are different from event to event, exhibiting a large variety of flow sequences while they seem to have repeated at a relatively narrow area over several tens of minutes. The present approach may be utilized for early detection and warning for prevention and reduction of the present type of disasters in the future.

© 2015 Elsevier B.V. All rights reserved.

1. Introduction

With recent construction of dense seismic networks at many regions over the world (e.g. High Sensitivity Seismograph Network Japan, Hi-net, Okada et al., 2004), seismic signals from not only ordinary earthquakes but also other natural and artificial phenomena have been clearly recorded. For example, Obara (2002) discovered deep low-frequency earthquakes or tremors on the plate boundary of the subducting Philippine Sea plate in southwest Japan. Because these low frequency earthquakes or tremors do not have any clear phase onset in records, Obara (2002) estimated locations of these signals with arrival time differences based on the envelope correlation among stations of Hi-net. Dense seismic networks recorded not only underground events but also surface and atmospheric events, such as landslides and meteoroid impacts, and analyses of seismic records for those events have been attempted (Ishihara et al, 2003; Yamada et al., 2012).

On the other hand, there are various types of seismic events observed at volcanic areas where a seismic network covers a relatively small area with high density. For most volcanic events, signals have no clear phase arrivals so that it used to be difficult to determine their hypocenters. Battaglia and Aki (2003) and Kumagai et al. (2010) estimated locations of seismic events in volcanic areas without clear phase arrivals, using only the information of the observed amplitude from these seismic signals. They utilized the spatial distribution of site-corrected seismic amplitudes under the assumption of virtually isotropic source radiation of high frequency due to strong scattering effects in volcanic areas. In addition, Kumagai et al. (2011) and Ogiso and Yomogida (2012) revealed migration of source locations during explosive events and volcanic tremors with the distribution of seismic amplitudes varying in time. Migration of source locations during pyroclastic flows (Yamasato, 1997; Jolly et al., 2002) and lahars (Kumagai et al., 2009) were also estimated with a similar approach, which is important for not only scientific aspects but also hazard reduction or early warning of such disasters.

Miharayama volcano located in the center of Izu-Oshima Island, which is in the south of Tokyo by 120 km, is one of the most active volcanoes in Japan. According to the eruption history summarized by Japan Meteorological Agency and the Volcanological Society of Japan (2013), eruptions of VEI = 2 or larger have occurred in about every 30–50 years since 1777. The last significant eruption (VEI = 3) occurred in 1986 when all the residents had to evacuate the island temporarily. Since then, no surficial eruptions have been observed. If we assume the above recent eruptive cycle to be applicable for the next eruption, it may occur within 10 to 30 years. Therefore a dense seismic network has been deployed on the island so as to detect any precursors of its eruption activity.

* Corresponding author.
E-mail address: mogiso@mri-jma.go.jp (M. Ogiso).

http://dx.doi.org/10.1016/j.jvolgeores.2015.03.015
0377-0273/© 2015 Elsevier B.V. All rights reserved.

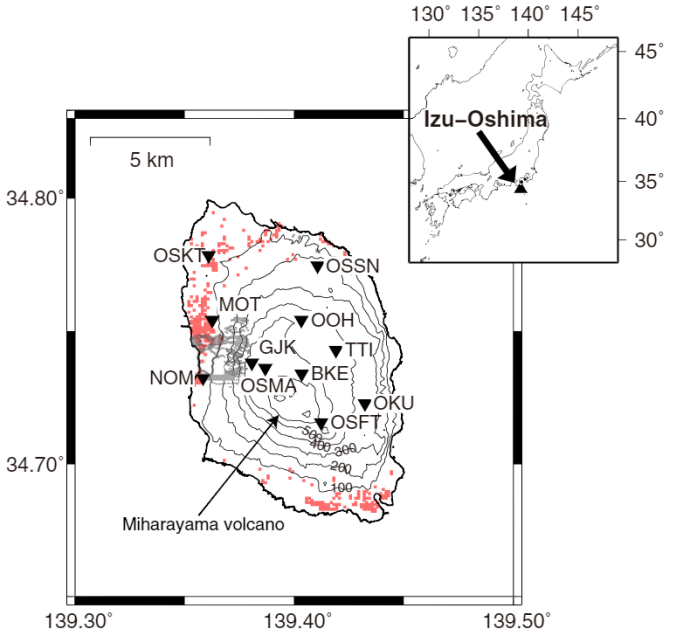

Fig. 1. Distribution of seismic stations on Izu-Oshima Island used in this study (inverted triangles) and the location of debris flow deposits investigated by aerial photographs (gray shaded area; after Geospatial Information Authority of Japan, 2013). We also plot areas of buildings for local residents by the red squares, based on the segmented mesh data of land utilization compiled by Ministry of Land, Infrastructure, Transport and Tourism, Japan.

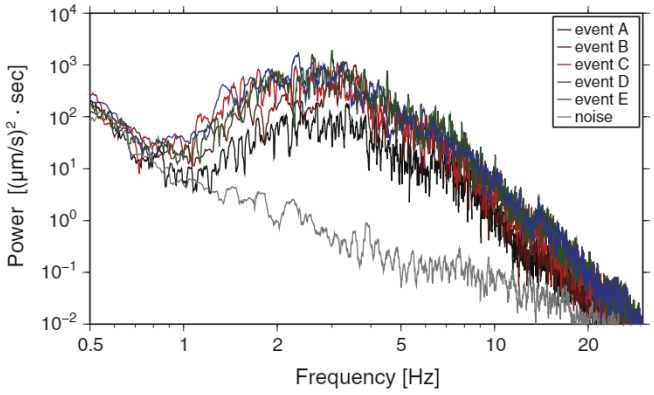

Fig. 3. Power spectra of five events and noise in vertical seismograms at station MOT.

On 16 October 2013, Typhoon 1326 (named Wipha) passed near the island, causing heavy rainfall there for a short time. This rainfall caused large-scale debris flows in the early morning of that day on the northwest flank of Miharayama volcano, resulting in 35 people dead and 4 people missing (Tokyo Metropolitan Government, 2013). Fig. 1 shows the distribution of debris flow deposits estimated later from aerial photographs (Geospatial Information Authority of Japan, 2013), together with the distribution of seismic stations on the island used in this study. We also plot areas of buildings based on the land utilization mesh data of the island, which may represent local residential areas. As shown in Fig. 1, the debris flows struck a highly inhabited region in the south of the station MOT. Many seismic stations recorded similar transient signals simultaneously, suggesting these signals originated from the debris flows. In this study, we estimate the source locations of these signals probably excited by the debris flows, and discuss the main features of flow sequences in that morning such as spatial and temporal migration processes.

2. Seismic signals from debris flows

Miharayama volcano on Izu-Oshima Island is one of the most active volcanoes in Japan, despite the relatively large population there (about 8000 residents in total). Because of the importance of monitoring its volcanic activity, Earthquake Research Institute of the University of Tokyo, the National Research Institute for Earth Science and Disaster Prevention, and the Japan Meteorological Agency have deployed seismic stations on Izu-Oshima Island intensively. As a result, a dense seismic network (spacing of about 2–3 km) is now constructed on the island, as shown in Fig. 1. Although there are some stations with both short-period and broadband seismometers, most of them are equipped only with a short-period of 1 s seismometer.

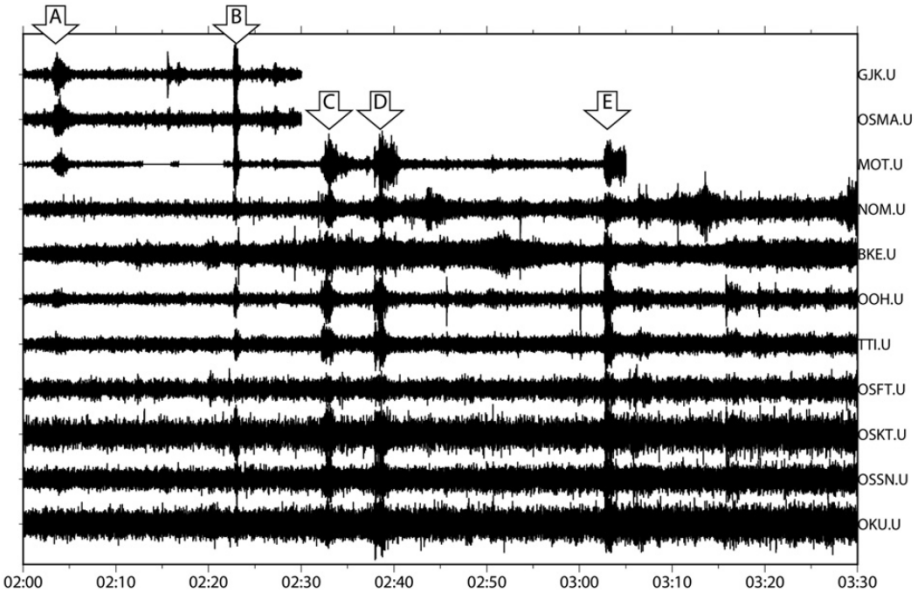

Fig. 2. Continuous vertical seismograms of 11 seismic stations with the names labeled in Fig. 1. Each trace is normalized by its maximum amplitude. Five noticeable events, named events A, B, C, D and E are indicated.

Table 1
List of the sets of stations on Izu-Oshima Island used for analysis of each event.

Event	Station
A	GJK MOT OOH OSMA
B	GJK MOT OOH OSKT OSMA TTI
C	MOT NOM OOH OSKT TTI
D	MOT NOM OOH OSKT TTI
E	BKE MOT NOM OKU OOH OSKT TTI
continuous (early part)	GJK MOT OOH OSFT OSKT OSMA OSSN TTI
continuous (later part)	BKE MOT NOM OKU OOH OSFT OSKT OSSN TTI

Large-scale debris flows occurred in the early morning on 16 October 2013, probably starting around 2:00 AM, according to the official disaster report of Tokyo Metropolitan Government (2013) based on its later survey. All the dates and times are referred to their local time called Japan Standard Time (9 h ahead of UTC) in this study. Fig. 2 shows continuous vertical waveforms of the seismic stations labeled in Fig. 1 from 2:00 to 3:30. In these records, there are several time windows when many stations recorded similar signals simultaneously, suggesting that these signals originated from common sources. At least five large events are identified in Fig. 2. We label them events A, B, C, D, and E in a chronological order. The duration time of each event is about 40 to 120 s. The power spectra of these events at station MOT are shown in Fig. 3. For comparison, we also show the power spectrum from 2:00:00 to 2:01:30 (90 s in duration) of small amplitudes as noise spectrum. The peak frequency of each event is about 2 to 4 Hz with a relatively common spectral shape. Each event clearly has larger power than noise between 2 and 10 Hz while the power below 1 Hz is almost the same as the noise power. In some previous studies, long-period seismic waves originated from landslides were observed, and their analysis based on conventional and deterministic source process revealed their properties (e.g. Kanamori and Given, 1982; Allstadt, 2013; Yamada et al, 2013). Several broadband seismometers on and around the island, however, recorded no clear long-period seismic signals, probably because the magnitude of the present debris flows was too small to have excited sufficient long-period signals. We focus only on high-frequency components of the recorded seismic signals. As mentioned in a later section, we shall select the frequency range from 5 to 10 Hz because the scattering effect of seismic waves in this frequency range is large enough to be able to assume isotropic source radiations in the analysis. In addition, the power in this frequency range is significantly larger than that of noise, as shown in Fig. 3.

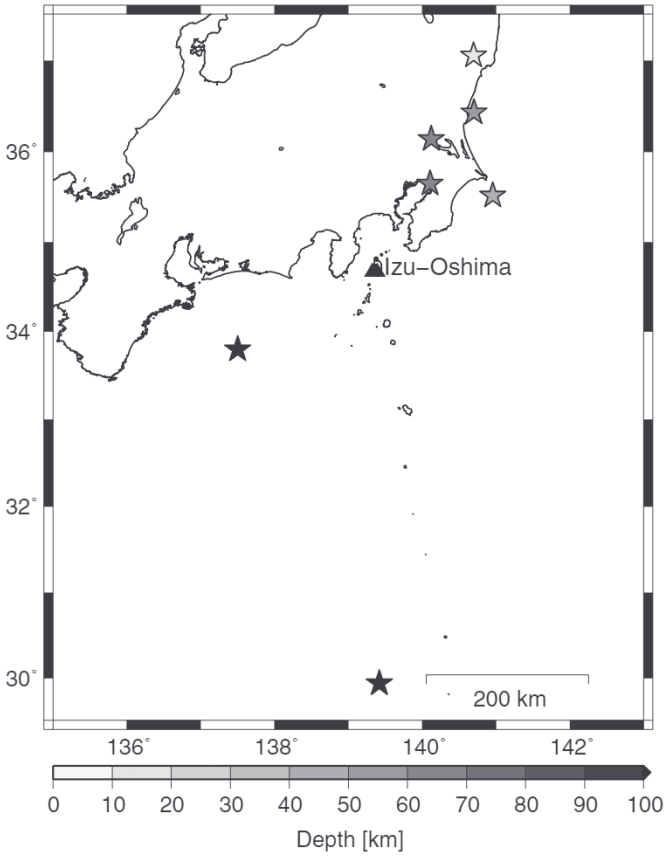

Fig. 4. Hypocentral distribution of the regional earthquakes used for the estimation of site amplification factors of stations on Izu-Oshima Island.

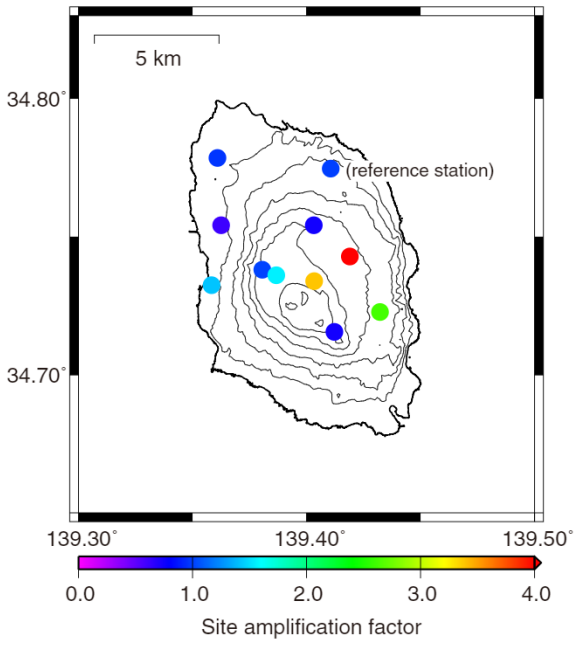

Fig. 5. Site amplification factors estimated at each station.

3. Method

The five seismic events identified in Fig. 2 have no clear onsets of P or S phase so that we cannot apply any conventional methods using phase arrival times to estimate the locations of these events. The envelope correlation method (ECM, Obara, 2002) is one of the effective methods to determine locations of such seismic events. ECM, however, works only for relatively long time windows to get high correlations in envelope among stations. On the other hand,

Table 2
List of the site amplification factors and their standard deviations of stations on Izu-Oshima Island. OSSN is selected as the reference station.

Station	Amplification factor	Standard deviation
BKE	3.3843	0.5433
GJK	1.0124	0.1670
MOT	0.6093	0.0851
NOM	1.4129	0.1965
OKU	2.6099	0.8397
OOH	0.7437	0.1015
OSFT	0.7392	0.2209
OSKT	0.9671	0.1220
OSMA	1.5550	0.2514
OSSN	1.0	(none)
TTI	12.6783	1.8489

the amplitude source location method, called by ASL (Yamasato, 1997; Jolly et al., 2002; Battaglia and Aki, 2003; Kumagai et al., 2010) uses only a spatial distribution of seismic amplitudes, and it can estimate a source location even with a narrow time window. As a result, ASL can also probe migration of source locations with high temporal resolution within volcanic events of a relatively short duration (Kumagai et al., 2011) or a monotonous signal such as continuous volcanic tremor (Ogiso and Yomogida, 2012). In this study, the five seismic events shown in Fig. 1 may be related to the debris flows mentioned in the previous section, so we focus on the locations of the five events within the duration time of each event (about 40 to 120 s), including their migration processes with the ASL approach.

ASL assumes that the seismic amplitude of body waves at frequency f observed at the i-th station, $A_i(f)$, is expressed by:

$$A_i(f) = A(f) \cdot \exp(-Br_i)/r_i \cdot S_i(f) \quad (1)$$

where $A(f)$ is the intensity of the source, r_i is the distance from the source to the i-th station, and $S_i(f)$ is the site amplification factor of

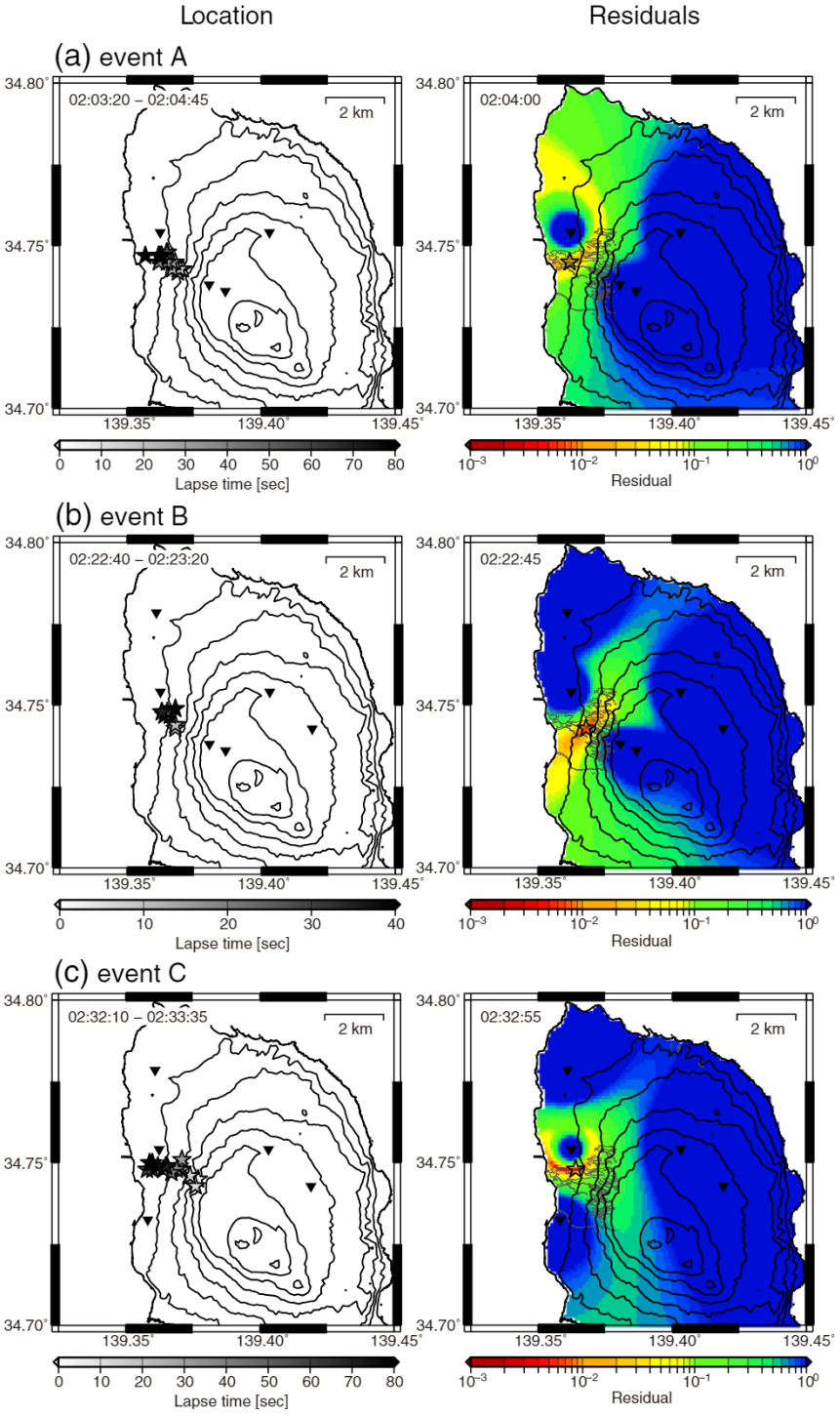

Fig. 6. Estimated locations (stars) in the left and residual distributions in the right when the source amplitude is maximum in each of five events: (a) event A, (b) event B, (c) event C, (d) event D and (e) event E. Colors of the stars are changed from white to black in correspondence with the lapse time from the beginning of each event. Inverted triangles indicate the seismic stations used for analysis of each event.

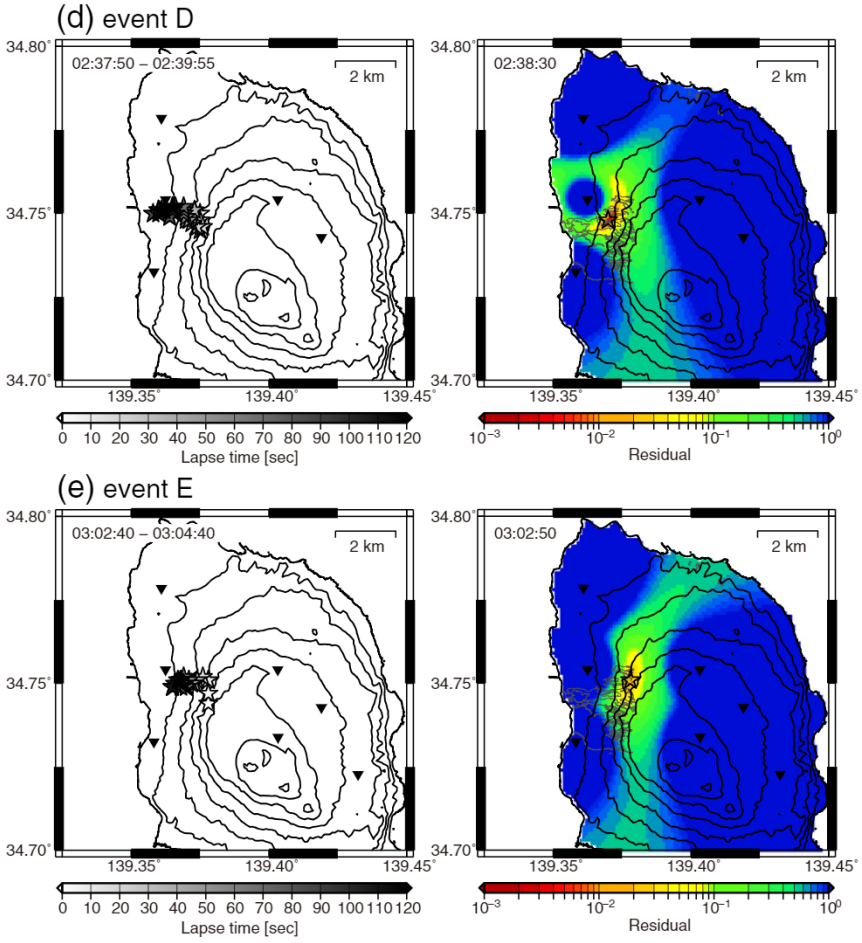

Fig. 6 (*continued*).

the i-th station. B represents the mean attenuation coefficient expressed by the quality factor Q and the average velocity of a medium β:

$$B = \pi f / Q\beta \tag{2}$$

After correcting the site amplification factor $S_i(f)$ estimated by independent data, we can calculate $A(f)$ from the total of N stations and an assumed source location as follows:

$$A(f) = \frac{1}{N}\sum_{i=1}^{N} A_i(f) r_i \exp(Br_i) \tag{3}$$

In general, a seismic source has a specific radiation pattern or strong azimuthal dependency so that the intensity at the source $A(f)$ depends on not only frequency but also the azimuthal relationship between source and station. Takemura et al. (2009) reported that the observed amplitude at high-frequency (above 5 Hz) does not show any clear radiation patterns, concluding that small-scale heterogeneities in the crust mask the original radiation pattern in comparison with numerical simulations of wave propagation. In addition, the strength of small-scale heterogeneities in a volcanic area is much stronger than non-volcanic ones (Yamamoto and Sato, 2010), so that we can take a reasonable assumption that the radiation pattern of source amplitude is virtually isotropic at frequency above 5 Hz for the data in this study.

In order to estimate the source location with the observed data, we define the following normalized residual:

$$residual \equiv \sum_{i=1}^{N} \{A_i(f) - A(f)\exp(-Br_i)/r_i\}^2 / \sum_{i=1}^{N} A_i^2(f) \tag{4}$$

We conduct a grid search with each assumed source location to find the minimum residual defined by Eq. (4). We do not need to search the intensity at the source $A(f)$ because it can be calculated by observed amplitudes at stations and Eq. (3) if we assume a source location. We limit the source locations assumed at the surface (i.e. depth of the source equals to the altitude of topography, referring to the digital elevation map) of the island, because each seismic signal are inferred to relate to the debris flow. That is, our source parameters to be searched are longitude and latitude only. We took the altitudes of the assumed source location and the i-th station into consideration in calculating its hypocentral distance r_i. Our grid in search is 0.001° in both longitudinal and latitudinal directions.

In this study, we calculate root-mean-square (RMS) amplitudes of waveforms with a time window of 10 s for the observed amplitude $A_i(f)$ in Eq. (1) or the other equations written above. Kumagai et al. (2010) pointed out that the time window for the RMS calculation should be shifted in time for each station, depending on the travel time of the supposed phase from the assumed source location to each station in order to archieve the location estimation with high resolution. We adopted such a time shift in calculating the RMS amplitude of each station.

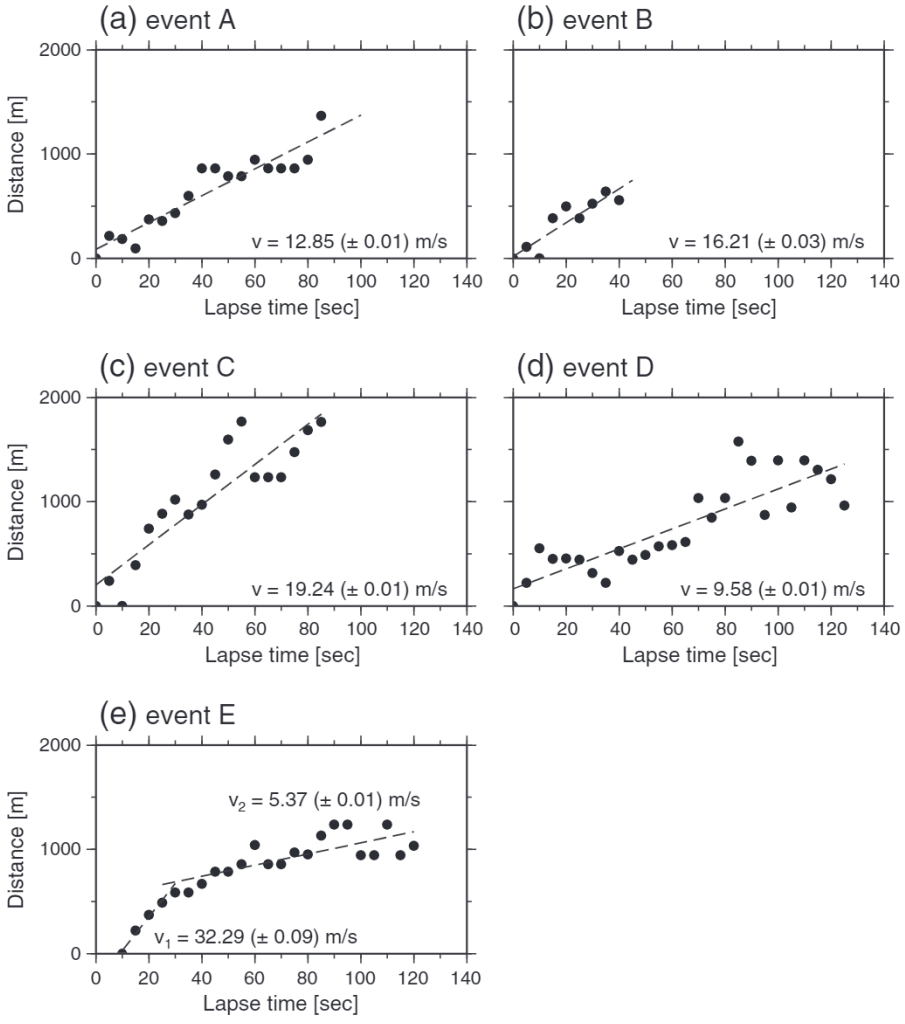

Fig. 7. Relationship of lapse time and migration distance, and estimated migration velocity during each of five events.

We apply a 5–10 Hz band pass filter to the observed seismograms before calculating the RMS amplitudes, that is, f is selected to be 7.5 Hz in the above equations. The power in this frequency range is abundant, as is shown in Fig. 3. In the frequency range of 5–10 Hz, the observed seismogram can be assumed to be composed of S body waves, but not surface waves because they are trapped in a very shallow part (shallower than one hundred meters) where intrinsic attenuation is very strong (e.g. Sato et al., 2012). This assumption was further confirmed in observational studies on volcanic areas (e.g. Yamamoto and Sato, 2010). We use 1.44 km/s for the velocity of the medium β in Eq. (2), referring to the velocity structure of Izu-Oshima Island estimated by Onizawa et al. (2002). We need to assume the value of Q in Eq. (2). Jolly et al. (2014) successfully employed the signals from artificial mass drops in the estimation of locations and other properties of natural phenomena without any assumptions of Q information. We do not, however, have any data from such active sources in this study. We therefore chose Q to be 100 and the effect of Q values will be discussed in a later section.

Prior to the application of the analytical method described above, we checked whether common signals were recorded or not at each station by careful visual inspection of the original and band-passed (5–10 Hz) waveforms for each event. Table 1 shows the list of stations that we used for each event in this study. All the data were recorded by short-period (1 s) seismometers. We used only vertical-component seismograms in this study, because of the possibility of large contamination of local noise particularly for horizontal components, such as short period surface waves due to severe weather conditions (intensive wind and rainfall) in the analyzed frequency range.

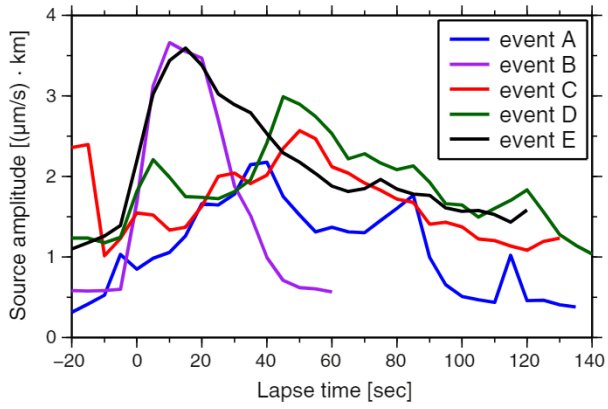

Fig. 8. Temporal variations of source amplitude during each event.

4. Site amplification factors

Site amplification factors play an important role in the ASL method (Kumagai et al., 2013). We used the coda normalization method

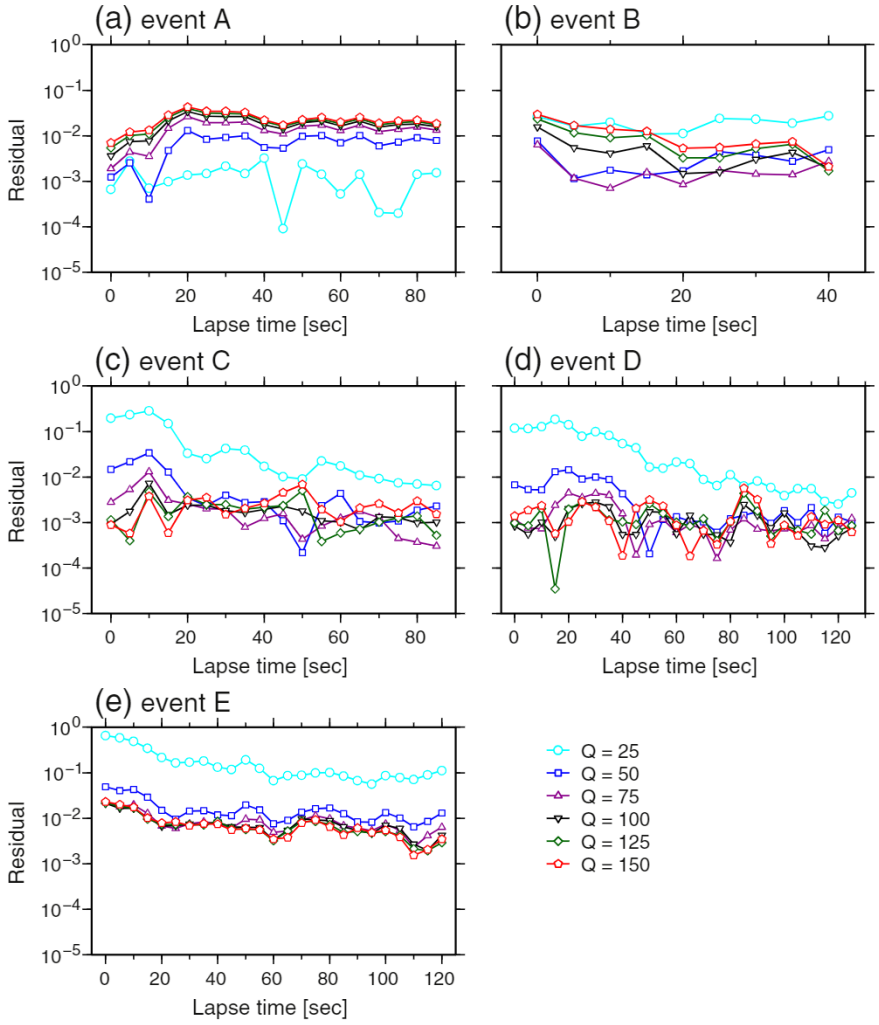

Fig. 9. Temporal variations of residuals for five events with six different values of Q.

(Phillips and Aki, 1986) to estimate the site amplification factor, $S_i(f)$, of each station. Coda waves, usually defined in the time window after twice as the travel time of the direct S wave, are composed of the waves backscattered by small-scale structural heterogeneities spread over a large area. As a result, the amplitude of coda waves mainly depends on its source intensity and site amplification factor with little effects of the mutual location of source and station, source radiation pattern and the incident direction to the station. The amplitude ratio of coda waves to a selected reference station for a given earthquake corresponds to the relative site amplification factor of each station.

At first, we selected seven regional earthquakes that occurred far enough from Izu-Oshima Island, as shown in Fig. 4. We calculated the travel time of direct P and S waves from the hypocenter to each station based on the information of the unified earthquake catalogue of the Japan Meteorological Agency and the JMA2001 travel time table (Ueno et al., 2002). Then we calculated the RMS amplitude of a 10 s time window just before its direct P arrival to define our noise level. Next, for the precise estimation of site amplification factors, we selected three time windows of 10 s. The first window started at twice as the travel time of the direct S wave. The second and third windows were shifted by 5 s and 10 s from the first window. We checked the signal levels of the three time windows by comparing the noise level defined above, and we excluded a time window if its signal-to-noise ratio was smaller than 3. Finally, we calculated the RMS amplitude ratio of each station with that of station OSSN as the reference station in each time window, and averaged the amplitude ratio of each station and time window for seven earthquakes to obtain the relative site amplification factor of each station. We selected OSSN because this station was installed in a borehole so that the signal-to-noise ratio seemed high.

The estimated site amplification factors of stations on Izu-Oshima Island used in this study are shown in Fig. 5, and their values are listed in Table 2. Amplification factors are under 2.0 in seven of eleven stations. High amplification factors are estimated for stations BKE and TTI. These two stations are located on the northeast side of the active crater so that their subsurface structures may be complicated due to the repeated eruption activities of the volcano.

5. Locations of five events

5.1. Locations estimation

After correcting the site amplification of each station estimated in the previous section, we estimated the locations of five events A, B, C, D, and E by minimizing the residual of Eq. (4). We set each time window of RMS amplitude calculations to be 10 s, shifting the center of the window by 5 s to cover the whole duration of each event ranging from 40 to 120 s.

Fig. 6 shows the estimated locations of the five events A, B, C, D, and E with each star at every 5 s. The color of stars varies from white to black as the time elapsing during each event. $Q = 100$ is assumed for these

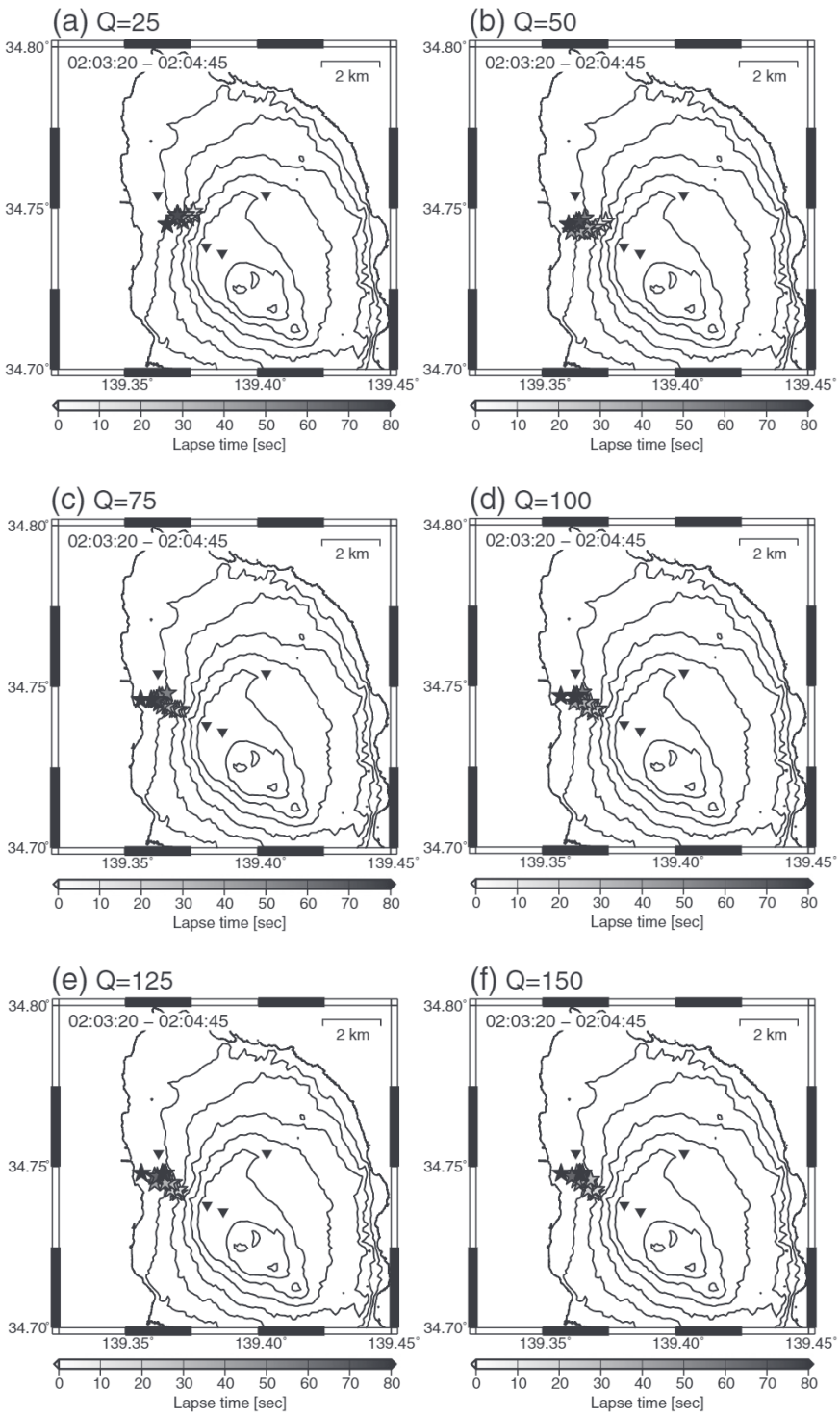

Fig. 10. Estimated source locations of event A with six different Q values. Stars are the estimated locations and the color of them corresponds to the lapse time of event A.

estimations. Fig. 6 also shows the spatial distributions of residuals defined by Eq. (4) as the measure of stability in our estimation for one time window in each event. The spatial spreads of residuals are about 1 km or smaller, which confirms our locations estimated by the data set and the present approach in this study to be reliable. That is, the signals of the five events in Fig. 2 can be concluded to correspond to some clear distinguished sources. The locations of all the events are estimated in the south of station MOT, where the debris flow deposits were identified, as shown in Fig. 1. Although we used different sets of stations in the analysis of the five events, all the estimated locations are well constrained in the area of the debris flow deposits. The locations are well constrained even for event A, the smallest of the five events, with which we could use only four stations of substantial signal levels.

One important feature common to all the events is the migration of source locations in the westward direction as the time passed, starting on a mountain side or close to the rim of Miharayama volcano. Due to the insufficient station distribution, source locations of events A (Fig. 6a) and B (Fig. 6b) seem to migrate in the NW direction compared with the west for the other three. Residual distributions of these two events are spread in the NE–SW direction, perpendicular to the

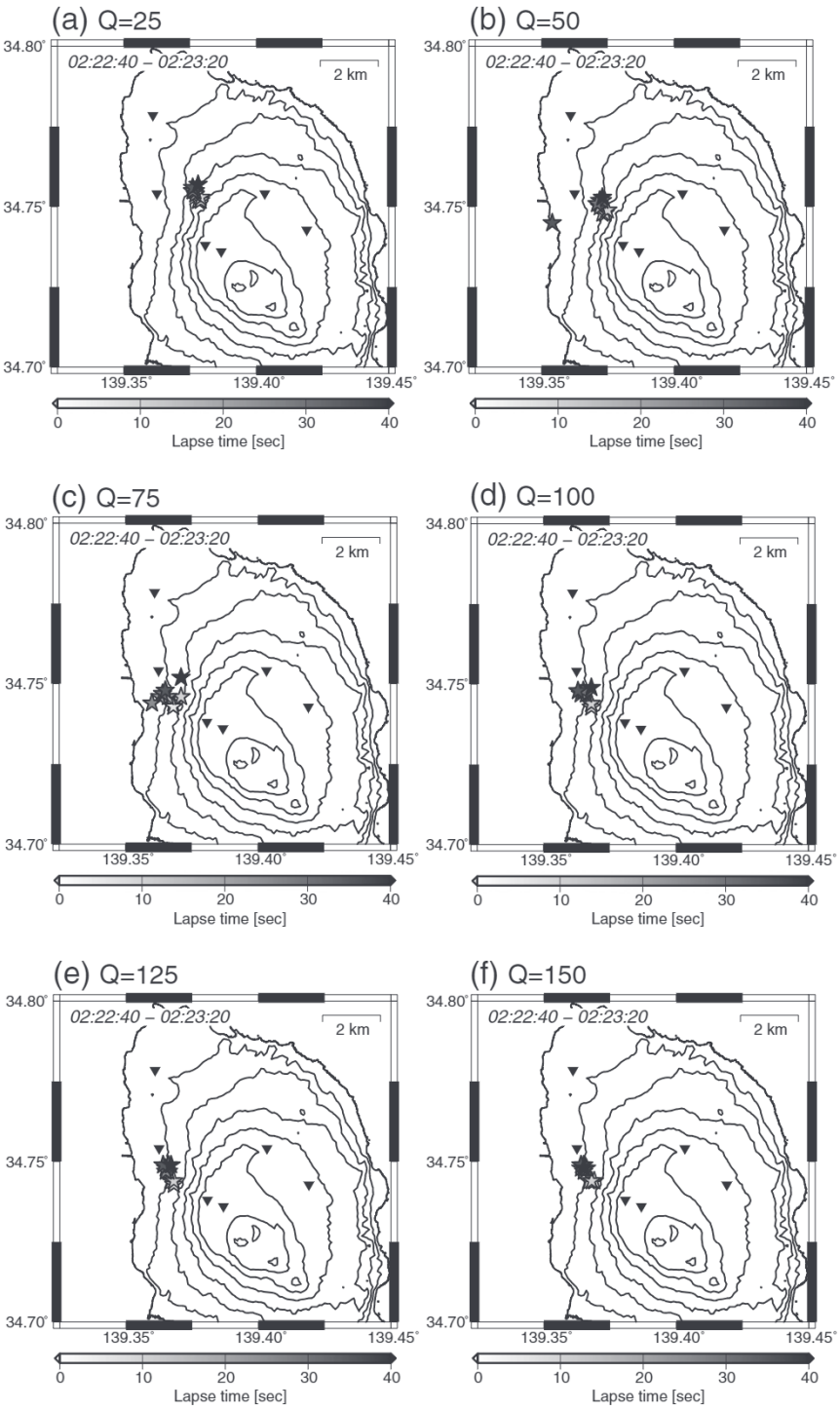

Fig. 11. Same as Fig. 10 except for the results of event B.

estimated migration direction of their source locations. This suggests that the migration of source locations during events A and B is not retrieved by random fluctuations of the observed amplitudes at each station but the relative locations between the beginning and ending of these events are changed systematically, although their absolute locations are affected by their insufficient station distribution. The extent of sources in the east–west direction is about 2 km or larger, except for less than 1 km for event B, the event of the shortest duration.

Since actual debris deposits flowed over areas from high altitude to low or from east to west in this case, the seismic signals of the five events are concluded to have originated from the debris flows, and the migration of source locations in each event can be considered to correspond to the flow process of each debris flow.

5.2. Spatial and temporal variations of source intensities during each event

As seen in Fig. 6, source locations appear to be changed in space significantly from east to west or to migrate during each event. In this section, we investigate the migration velocity of their relative locations in each event, because it is important for the interpretation of debris flow sequences.

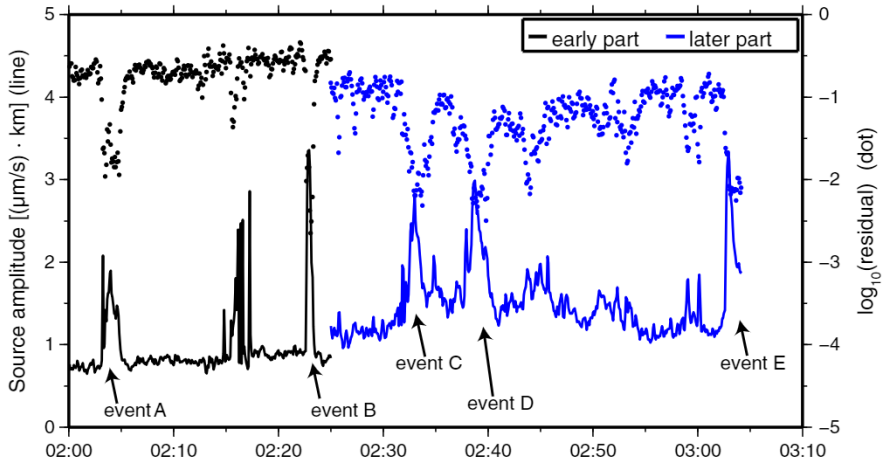

Fig. 12. Temporal variations of source amplitude (solid line) and minimum residual (dots) when we applied the ASL method to continuous records from 2:00 to 3:05.

We set the origin of locations as the one estimated at the lapse time of 0 s for each event. For event E, however, its origin is set to be the location at the lapse time of 10 s, because locations at the lapse times before 5 s are estimated to be slightly shifted in the south of later locations (see Fig. 6e). We then calculate the distance from the origin to the source location estimated at each later time window. Fig. 7 shows the relation between lapse time and migration distance for each event. We fit a linear function to each relation in a least-square sense. A linear function explains it well except for event E. The estimated average velocities or migration velocities are about 13, 16, 19, and 10 m/s for events A, B, C and D, respectively. For event E, two different behaviors are clearly seen before and after 30 s, as shown in Fig. 7(e): the velocity is about 32 m/s before 30 s while 5 m/s, a much smaller value, for its later part. Although locations of all the five events are estimated to be in a nearly same place, the migration velocities are quite different from each other as well as their total duration times ranging from 40 s to 120 s. These results should reflect a high level of diversity in dynamic process of the present debris flows. For event E, particularly, migration velocity was suddenly reduced around 30 s. We interpret that the initiation of event E at 3:02:50 was violent but its flow was slowed down as it fell into the downstream on about 600 m west of its initiation point at 3:03:10, or 20 s after its initiation time.

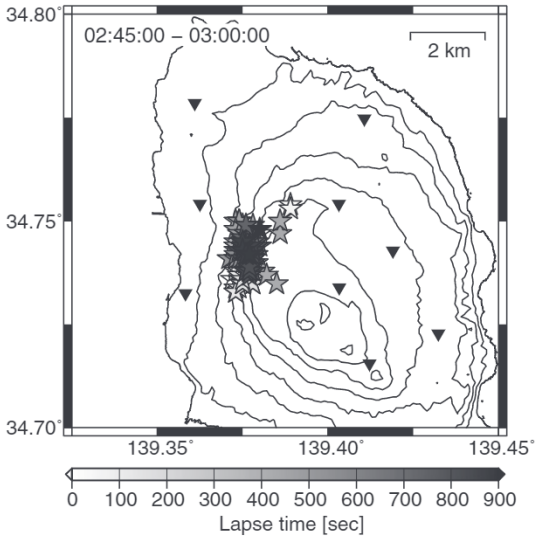

Fig. 13. Estimated locations (stars) of continuous records between 2:45 and 3:00 and the stations used in the analysis (inverted triangle). Colors of the stars are changed from white to black in correspondence with the lapse time from 2:45.

During each event, the intensity or amplitude at the source $A(f)$ in Eq. (1) was also varied significantly. Fig. 8 shows the temporal variations of source amplitude during the five events. An emergent increase of source amplitude was seen just after each origin time for events B and E, while the amplitudes of the other three events gradually increased as time elapsed. Their temporal decay rates are similar to each other except for event B of a significantly short duration. Clearly different behavior is noticeable for event B, characterized by its abrupt termination at the lapse time of 40 s. Its early part of 20 s is similar to event E, but its later decay curve is quite different. A gentle decay of amplitude after 30 s in event E corresponds to its sudden drop of migration velocity from 30 m/s to 5 m/s, as mentioned above in Fig. 7(e). In other words, the second or later stage may be added to the process of event B to yield the entire process of event E.

Despite the similarity in the decay curve of source amplitude in Fig. 8, the migration velocity of the later part of event E is significantly slower than the other three events A, C, and D, suggesting that event E has a unique flow process. Future investigations are required to understand the detailed mechanism that caused the diversity in migration velocity and temporal variation of source amplitude even though these flows took place repeatedly at a nearly common location.

5.3. Effect of the choice of Q values

We discussed the diversity of debris flow processes in the previous section, fixing the Q value to be 100. In the ASL method, however, the assumed Q value may affect our source location estimation. In order to check whether our estimation of source locations in the previous section was biased or not, we tested five cases with different Q values ($Q = 25$, 50, 75, 125, and 150) for each event. Fig. 9 shows the temporal variations of residuals with the five different Q values as well as the case of $Q = 100$. Although the result of $Q = 25$ for event A (Fig. 9a) shows small residuals than those of large Q values, the other four events give large residuals in the case of $Q = 25$. If Q is larger than 50, there are no significant differences in temporal variation of residuals.

We show the estimated source locations of events A and B in the case of six different Q values in Figs. 10 and 11, respectively. Same as Fig. 6, each star represents the location estimated in a time window shifted by 5 s, and its color varies from white to black as the time elapsing during each event. The source locations estimated with small Q values tend to be converged or estimated at similar locations, compared with the results with large Q values. With a very small value of Q, the exponential factor in Eq. (1) becomes dominant over the term of the inverse

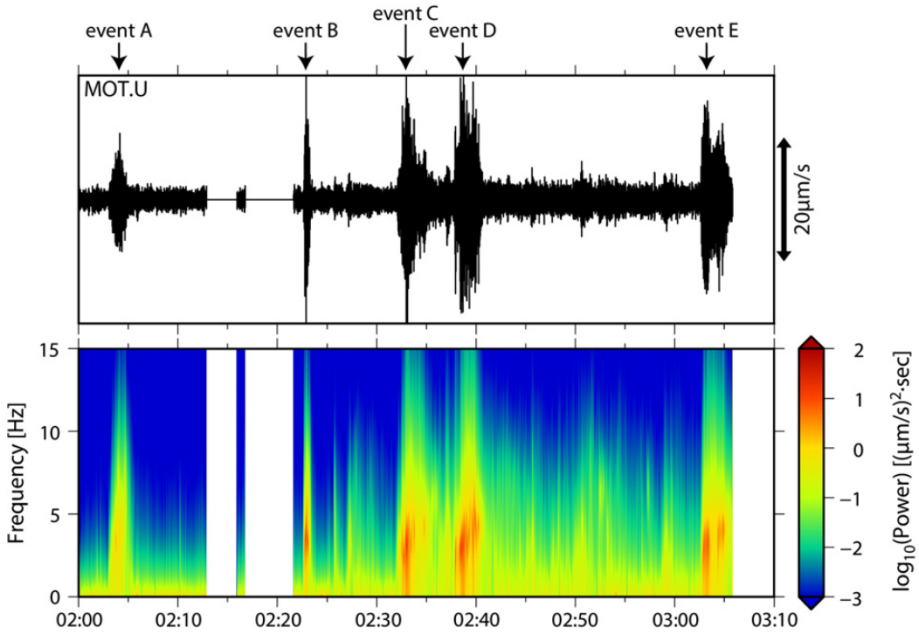

Fig. 14. Observed waveform of vertical component and its running spectra at station MOT from 2:00:00 to 3:05:48.

of distance, reducing the sensitivity of source locations to the relative change of the observed amplitudes. As a result, the locations with a small Q value are concentrated in space, as shown in Figs. 10 and 11.

Figs. 9–11 show that both residuals and estimated locations do not change so much if Q is larger than 100, suggesting that these results seem to be stable. In this study, the seismic signals correspond to the debris flow sequences, and we know that their locations covered an area over 2 km from the other surveys (e.g. Geospatial Information Authority of Japan, 2013, Fig. 1) after the disaster occurred. The area covering the estimated locations with $Q \geq 100$ is consistent to this actual flow area, which also supports the validity of Q to be larger than 100. Because we do not find any clear evidence that Q should be less than 50 for S wave at frequency of 5–10 Hz in this region, we can conclude that the results obtained with the choice of $Q = 100$ adopted in this study are reasonable, and its choice affects the estimated locations of debris flows very weakly in practice.

6. Possibility of detection of flow sequences without clear seismic signals

We have analyzed five events whose seismic signals are clearly noticeable in continuous waveforms of Fig. 2. Since the amplitude of seismic signals depends on their magnitude or intensity, signals from debris flows smaller than the five events may be hidden in continuous records rich in background noise. By visual inspection of continuous waveforms of Fig. 2, it is hard to identify any of such signals except for the five events.

Several witnesses reported the damage caused by flows at the timings not always corresponding to the five large events that we retrieved (Kajiya, personal communication). Although the accuracy of timings of these human reports should have a large degree of uncertainties, it is natural that not only five large debris flows occurred on that day, but there were also many small debris flows among them. Since the ASL method can be applied to a record section of continuous seismograms without any clear signals in principle, we attempt to investigate the feasibility to detect such small flow sequences.

In the analysis of continuous records starting at 2:00, we divided the whole record section into two parts before and after 2:25 because we had to use different sets of stations. Continuous records at station GJK and OSMA were missed after 2:30 (see Fig. 2 and Table 1), due to the failure of their communication lines.

Fig. 12 shows temporal variations of source amplitude and minimum residual when we applied the ASL method to the continuous records from 2:00 to 3:05. The condition of calculations is the same as that of the previous sections for the five events, except for the sets of stations, as listed in Table 1.

Five timings of large source amplitudes which we already discussed are seen in Fig. 12. Around 2:15 or between events A and B, there is a clear part of large source amplitude and small residual. This possible minor event can also be identified visually in some of continuous records such as GJK and OSMA, as shown in Fig. 2. This minor event may have occurred near GJK and OSMA with small magnitude.

Between events D and E, there are several timings of large source amplitude and small residual in spite of no noticeable signals in continuous records of Fig. 2. Fig. 13 shows the estimated source location of the time window at every 5 s between 2:45 to 3:00. All the estimated sources are located on the upper or mountain side of the area of the debris flow deposits. No systematic temporal patterns of migration from the mountain side to the ocean site are recognized in this case, dissimilar to the five events, suggesting no systematic or coherent flows over 2 km in distance.

Fig. 14 shows running spectra of records at station MOT, covering the period of Fig. 12. The waveform at MOT has a certain level of power at frequency higher than 1 Hz at the timings of possible minor flows between events D and E, whose frequency contents are not found in noise parts, as shown in Fig. 3. It is possible that this high frequency power between events D and E may be originated from small but plural debris flows. We have to check carefully whether the estimated locations of the continuous record section in Fig. 13 are consistent with other evidence of small-scale debris flows or just artifacts due to the limited distribution of stations and background noise. Nevertheless, the present ASL method seems to detect the meaningful signals even though they are not identified in the waveforms visually.

7. Conclusions

We analyzed the seismic signals associated with large debris flow sequences on Izu-Oshima Island between 2:00 to 3:05 on 16 October 2013. Source locations of five large events were estimated to be in the

south of station MOT, where debris flows indeed caused severe damage. We also found source migration during each event, and its migration velocity was relatively constant within each event but varied from 10 m/s to 20 m/s among events, except for event E, where the velocity suddenly decreased from 30 m/s to 5 m/s at 20 s after its initiation time. Comparison of temporal variations of source amplitude showed some degrees of similarity and differences among events. Source amplitudes of events B and E emergently increased in a common temporal feature, but their later behaviors were quite different: sudden decay of source amplitude for event B while gentle and long decay for event E. In addition, we showed the feasibility to detect small-scale debris flows whose seismic signals were not clearly distinguished from background noise in waveforms.

Using the ASL method in this study, seismic signals from debris flows enable us to detect their occurrence and to estimate their locations without visual observations. That is, the present approach is effective at not only daytime but also nighttime or during severe weather conditions such as heavy rainfall. Moreover, the estimation of the migration of source locations will help us with the monitoring of flow direction. Although we have to check the accuracy and reliability of the ASL method in detail to understand the variability of debris flow sequences, the ASL method can be extended to a real-time observation and a warning system for debris flows or similar kinds of natural disasters in the future.

Acknowledgments

We thank the staff of Earthquake Research Institute of the University of Tokyo, the National Research Institute for Earth Science and Disaster Prevention, and the Japan Meteorological Agency (JMA) for the permission for us to use their seismic records and their long-time efforts to maintain their seismic networks on Izu-Oshima Island. Akimi Kajiya kindly provided us with the witness evidence of local residents about the disaster. We used the unified hypocenter catalogue maintained by JMA in cooperation with the Ministry of Education, Culture, Sports, Science and Technology, Japan. We also used the digital data of coastlines, elevations and distribution areas of debris flow deposits compiled by the Geospatial Information Authority of Japan. The segmented mesh data of land utilization was made by the Ministry of Land, Infrastructure, Transport and Tourism, Japan. Comments by two anonymous reviewers significantly improved the manuscript. Figures in this paper were drawn by GMT (Wessel and Smith, 1998).

References

Allstadt, K., 2013. Extracting source characteristics and dynamics of the August 2010 Mount Meager landslide from broadband seismograms. J. Geophys. Res. Earth Surf. 118. http://dx.doi.org/10.1002/jgrf.20110.

Battaglia, J., Aki, K., 2003. Location of seismic events and eruptive fissures on the Piton de la Fournaise volcano using seismic amplitudes. J. Geophys. Res. 108 (B8). http://dx.doi.org/10.1029/2002JB002193.

Geospatial Information Authority of Japan, 2013. Public release of aerial photographs showing disaster areas damaged from a landslide caused by heavy rain due to typhoon No.26, 2013. http://www.gsi.go.jp/kokusaikoryu/kokusaikoryu-e30023.html (Last accessed: 16, Sep., 2014).

Ishihara, Y., Tsukada, S., Sakai, S., Hiramatsu, Y., Furumoto, M., 2003. The 1998 Miyako fireball's trajectory determined from shock wave records of a dense seismic array. Earth Planets Space 55, e9–e12.

Japan Meteorological Agency and the Volcanological Society of Japan, 2013. Izu-Oshima, on National catalogue of the active volcanoes in Japan (the fourth edition, English version). http://www.data.jma.go.jp/svd/vois/data/tokyo/STOCK/souran_eng/volcanoes/058_izu-oshima.pdf (Last accessed: 17, Jan., 2015).

Jolly, A.D., Thompson, G., Norton, G.E., 2002. Locating pyroclastic flows on Soufriere Hills Volcano, Montserrat, West Indies, using amplitude signals from high dynamic range instruments. J. Volcanol. Geotherm. Res. 118, 299–317.

Jolly, A.D., Lokmer, I., Kennedy, B., Keys, H.J.R., Proctor, J., Lyons, J.J., Jolly, G.E., 2014. Active seismic sources as a proxy for seismic surface processes: an example from the 2012 Tongariro volcanic eruptions, New Zealand. J. Volcanol. Geotherm. Res. 286, 317–330. http://dx.doi.org/10.1016/j.jvolgeores.2014.04.008.

Kanamori, H., Given, J.W., 1982. Analysis of long-period seismic waves excited by the May 18, 1980 eruption of Mount St. Helens—a terrestrial monopole? J. Geophys. Res. 87 (B7), 5422–5432.

Kumagai, H., Palacios, P., Maeda, T., Castillo, D.B., Nakano, M., 2009. Seismic tracking of lahars using tremor signals. J. Volcanol. Geotherm. Res. 183, 112–121. http://dx.doi.org/10.1016/j.jvolgeores.2009.03.010.

Kumagai, H., Nakano, M., Maeda, T., Yepes, H., Palacios, P., Ruiz, M., Arrais, S., Vaca, M., Molina, I., Yamashina, T., 2010. Broadband seismic monitoring of active volcanoes using deterministic and stochastic approaches. J. Geophys. Res. 115 (B08303). http://dx.doi.org/10.1029/2009JB006889.

Kumagai, H., Placios, P., Ruiz, M., Yepes, H., Kozono, T., 2011. Ascending seismic source during an explosive eruption at Tungurahua volcano, Ecuador. Geophys. Res. Lett. 38, L01306. http://dx.doi.org/10.1029/2010GL045944.

Kumagai, H., Lacson, R., Maeda, Y., Figueroa, M.S., Yamashina, T., Ruiz, M., Palacios, P., Ortiz, H., Yepes, H., 2013. Source amplitudes of volcano-seismic signals determined by the amplitude source location method as a quantitative measure of event size. J. Volcanol. Geotherm. Res. 257, 57–71.

Obara, K., 2002. Nonvolcanic deep tremor associated with subduction in southwest Japan. Science 296, 1679–1681. http://dx.doi.org/10.1126/science.1070378.

Ogiso, M., Yomogida, K., 2012. Migration of tremor locations before the 2008 eruption of Meakandake Volcano, Hokkaido, Japan. J. Volcanol. Geotherm. Res. 217–218, 8–20. http://dx.doi.org/10.1016/j.jvolgeores.2011.12.005.

Okada, Y., Kasahara, K., Hori, S., Obara, K., Sekiguchi, S., Fujiwara, H., Yamamoto, A., 2004. Recent progress of seismic observation networks in Japan—Hi-net, F-net, K-NET and KiK-net—. Earth Planets Space 56, xv–xviii.

Onizawa, S., Mikada, H., Watanabe, H., Sakashita, S., 2002. A method for simultaneous velocity and density inversion and its application to exploration of subsurface structure beneath Izu-Oshima volcano, Japan. Earth Planets Space 54 (803–817), 2002.

Phillips, S., Aki, K., 1986. Site amplification of coda waves from local earthquakes in central California. Bull. Seismol. Soc. Am. 76, 627–648.

Sato, H., Fehler, M.C., Maeda, T., 2012. Seismic Wave Propagation and Scattering in the Heterogeneous Earth. Second edition. Springer (496 pp.).

Takemura, S., Furumura, T., Saito, T., 2009. Distortion of the apparent S-wave radiation pattern in the high-frequency wavefield: Tottori-Ken Seibu, Japan, earthquake of 2000. Geophys. J. Int. 178, 950–961. http://dx.doi.org/10.1111/j.1365-246X.2009.04210.x.

Tokyo Metropolitan Government, 2013. News of disaster prevention (FY 2013). http://www.bousai.metro.tokyo.jp/saigai/1000036/1000802/1000231.html (In Japanese, last accessed: 16, Sep., 2014).

Ueno, H., Hatekeyama, S., Aketagawa, T., Funasaki, J., Hamada, N., 2002. Improvement of hypocenter determination procedures in the Japan Meteorological Agency. Q. J. Seismol. 65, 123–134 (In Japanese).

Wessel, P., Smith, W.H.F., 1998. New, improved version of the Generic Mapping Tools released. Eos. Trans. AGU 79, 579.

Yamada, M., Matsushi, Y., Chigira, M., Mori, J., 2012. Seismic recordings of landslides caused by Typhoon Talas (2011), Japan. Geophys. Res. Lett. 39. http://dx.doi.org/10.1029/2012GL052174 L13301.

Yamada, M., Kumagai, H., Matsushi, Y., Matsuzawa, T., 2013. Dynamic landslide processes revealed by broadband seismic records. Geophys. Res. Lett. 40, 2998–3002. http://dx.doi.org/10.1002/grl.50437.

Yamamoto, M., Sato, H., 2010. Multiple scattering and mode conversion revealed by an active seismic experiment at Asama volcano, Japan. J. Geophys. Res. 115, B07304. http://dx.doi.org/10.1029/2009JB007109.

Yamasato, H., 1997. Quantitative Analysis of Pyroclastic Flows Using Infrasonic and Seismic Data at Unzen Volcano, Japan. J. Phys. Earth 45, 397–416.